ELSEVIER

Journal of Materials Processing Technology 166 (2005) 79–85

Journal of Materials Processing Technology

www.elsevier.com/locate/jmatprotec

In situ synthesis of AlN in Mg–Al alloys by liquid nitridation

H.Z. Ye*, X.Y. Liu, Ben Luan

Integrated Manufacturing Technologies Institute, National Research Council of Canada, London, ON, Canada N6G 4X8

Received 9 February 2004; received in revised form 21 June 2004; accepted 30 June 2004

Abstract

This paper reports the results of an investigation on the in situ formation of AlN particles in a Mg–Al alloy through liquid nitridation. The AlN particles were produced in the Mg–Al melt by bubbling nitrogen gas through the molten alloy. The key mechanism of AlN formation is the combined reactions of $3Mg + N_2 \rightarrow Mg_3N_2$ and $Mg_3N_2 + 2Al \rightarrow 2AlN + 3Mg$.

Keywords: Magnesium; Composite; AlN; Liquid nitridation; In situ particle formation; Casting

1. Introduction

Magnesium matrix composites have attracted increasing attention as light-weight engineering materials in recent years because they offer a unique combination of mechanical properties that are difficult or impossible to obtain from monolithic magnesium alloys. Conventionally, magnesium matrix composites, reinforced with various ceramic particles such as SiC, TiC, and AlN, are fabricated through stir casting [1], squeeze casting [2], or powder metallurgy [3]. However, these fabrication processes usually require expensive reinforcement materials and involve complex equipment and procedures, thus imposing a relatively high cost. An alternative route for cost-effective fabrication of metal matrix composites is in situ synthesis method developed in recent years. This method offers a number of attractive features, such as good reinforcement/matrix compatibility, homogeneous distribution of the reinforcing particles, and potentially low cost. To date, several magnesium matrix composites have been fabricated using the in situ method, including Mg_2Si/Mg, MgO/Mg, TiC/Mg, and (TiB_2–TiB)/Mg composites synthesized from Mg–Si [4–6], Mg–B_2O_3 [7], Mg–Ti–C [8], and Mg–KBF_4–K_2TiF_6 [9] systems, respectively.

Among the various in situ fabrication methods, liquid nitridation has proved to be a promising technique for the formation of aluminum matrix composite with AlN reinforcement [10–13]. The process is carried out by nitriding molten Al–Mg alloy in N_2 gas under controlled conditions. Two different AlN formation mechanisms have been identified in such a nitridation process of a molten Al–Mg alloy: the direct nitridation is achieved through the reaction, $2Al + N_2 \rightarrow 2AlN$; and the indirect nitridation realized through the formation of an intermediate phase of Mg_3N_2 through the reactions, $3Mg + N_2 \rightarrow Mg_3N_2$, followed by $Mg_3N_2 + 2Al \rightarrow 2AlN + 3Mg$. The liquid nitridation process is simple to implement and requires no expensive reinforcement materials. The formation of AlN is accelerated with increasing Mg content, N_2 pressure, and melting temperature. Depending on the processing parameters, three forms of AlN can be formed in situ, including a dense layer, dispersed particles, and pure AlN ceramics [10]. The presence of magnesium in molten aluminum is essential for the formation of AlN, and formation temperature decreases with an increase in magnesium content. Serving as a catalyst during the process, magnesium is vaporized and reacts with N_2 gas to form Mg_3N_2 particles in the gaseous state. The Mg_3N_2 particles subsequently fall into the Al melt, generating AlN phases by a displacement reaction. When the concentration of magnesium in the Al–Mg melt goes below a certain value, however, the magnesium vapor pressure becomes too low to trigger the indirect nitridation process, and nitridation mainly takes place by the direct route. Unfortunately, this direct nitridation process cannot significantly proceed because of surface passivation [11].

* Corresponding author. Tel.: +1 519 430 7157; fax: +1 519 430 7064.
E-mail address: haizhi.ye@nrc.gc.ca (H.Z. Ye).

0924-0136/$ – see front matter.
doi:10.1016/j.jmatprotec.2004.06.033

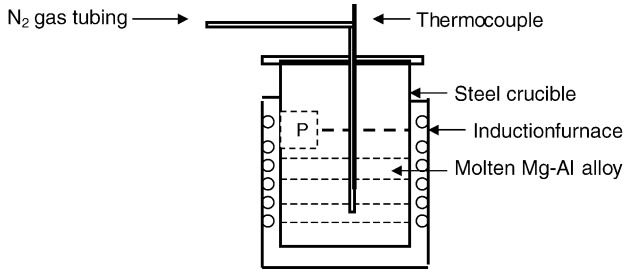

Fig. 1. Schematic of experimental setup for melting.

Whether or not similar liquid nitridation reactions occur in Mg–Al alloys has not been investigated. The Mg–Al alloys have a much higher Mg concentration but a lower Al content as compared to the Al–Mg alloys. Thermodynamically, it can be inferred that the reaction of $3Mg + N_2 \rightarrow Mg_3N_2$ is more favorable while the tendency for the reactions of $2Al + N_2 \rightarrow 2AlN$ and $Mg_3N_2 + 2Al \rightarrow 2AlN + 3Mg$ may be reduced in the Mg–Al alloys. In a recent study on in situ formation of AlN particles in a Mg–10% Al alloy with externally added Mg_3N_2 powders, the existence of the reaction of $Mg_3N_2 + 2Al \rightarrow 2AlN + 3Mg$ in the molten magnesium alloy was confirmed by the present authors [14]. Thus, the indirect liquid nitridation seems to be workable in Mg–Al alloy, which may provide a novel approach to in situ form AlN reinforcement for magnesium matrix composite. In this paper, results from our recent investigations are presented to discuss the forming behavior of AlN in a Mg–Al alloy through liquid nitridation.

2. Experimental procedures

An AM60B magnesium alloy was chosen as the base material. The aluminum content was varied between 6 wt.% and 15 wt.% to examine its effect on AlN formation at a melting temperature of 700 °C. Melting was performed in a vacuum induction furnace, as schematically shown in Fig. 1. The effect of melting temperature on the formation of AlN was also investigated by melting a Mg–12.5 wt.% Al alloy at 620 °C, 700 °C and 800 °C. The furnace was initially evacuated to 9.3×10^{-2} Pa and subsequently backfilled with N_2 gas to 3.3×10^4 Pa before melting. After the ingot was melted, N_2 gas was bubbled into the melt through a 304 stainless steel tubing for 1 h. The molten alloy was then poured into a receiving steel crucible and solidified into an ingot for characterization.

The microstructure of the as-cast samples was examined using an Olympus PMG3 optical microscope (without etching) and a Hitachi S-3500 scanning electron microscope (SEM) with energy-dispersive spectrometer (EDS). The samples were also subjected to X-ray diffraction analysis using a Philips X'pert X-ray diffractometer.

3. Experimental results

3.1. The effects of melting temperature

3.1.1. The formation of Mg_3N_2

During melting, a thin layer of green powder was observed on the wall and the cover of the melting crucible after the N_2 gas was bubbled into the magnesium melt. The amount of the green powder, however, was found to change with the melting temperature. At 800 °C, a significant amount of green powder was observed. However, when the melting temperature was lowered to 700 °C, only a thin film of green powder was formed, and, at 620 °C, no green powder was observed. X-ray diffraction was conducted to understand the phase composition of the green powder. From the result shown in Fig. 2, the major phase of the green powder was identified to be Mg_3N_2. These results showed that, under the given processing conditions, Mg_3N_2 powder was formed in the gaseous phase when the melt temperature was above 620 °C; and the formation tendency of the Mg_3N_2 powder increased with increasing melt temperature.

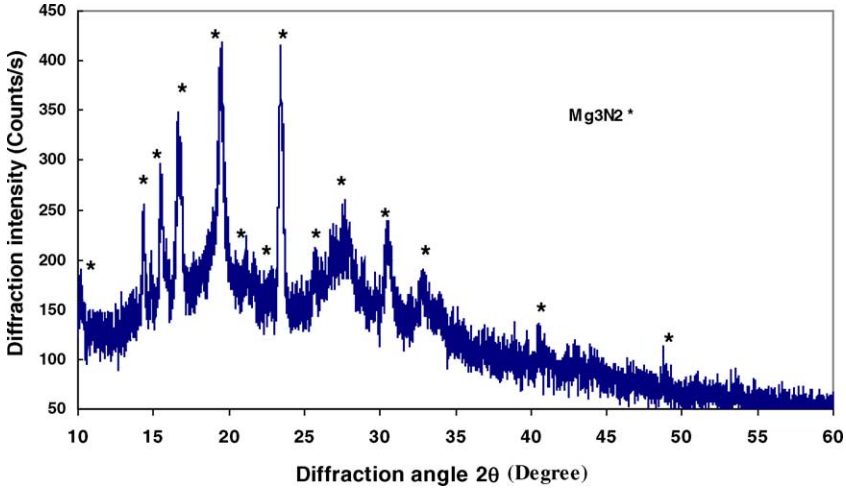

Fig. 2. XRD pattern (Mo Kα) of the green powder produced during melting of Mg–12.5 wt.% Al at 700 °C.

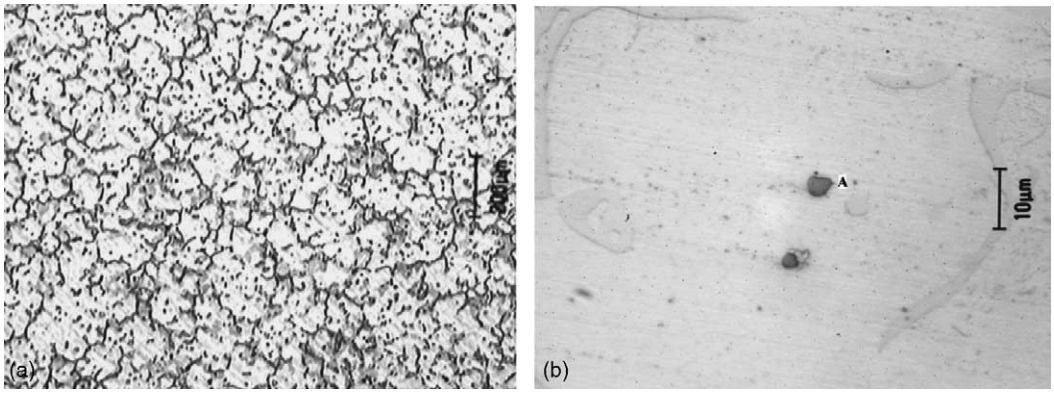

Fig. 3. Optical micrographs of the Mg–12.5 wt.% Al sample melted at 620 °C.

3.1.2. Microstructure

The microstructure of the samples melted at 620 °C consists of primary magnesium grains with isolated particles distributed in the matrix, as shown in Fig. 3. The composition of the isolated particles (labeled as A in Fig. 3b) was analyzed by EDS. The results revealed that these particles contained mainly Mg, Al, and Mn, along with a small amount of Ni, as shown in Table 1. The particle-free areas had an average composition of 92.1 wt.% Mg–7.9 wt.% Al.

The optical micrographs for the samples melted at 700 °C are shown in Fig. 4. Compared to the samples melted at 620 °C, a greater amount of particles were formed with significant segregation. The particles, (labeled as A in Fig. 4b) had irregular shapes with a maximum size of a few microns. A fibre-like microstructure (labeled as B in Fig. 4b) was also present in the particle-segregated area. The EDS analysis showed that the composition of these particles is similar to that of the particles in the samples melted at 620 °C, and the particle-free areas had an average composition of 91.9 wt.% Mg–8.1 wt.% Al.

When melted at 800 °C, a portion of the melt solidified on the top wall of the melting crucible, as schematically shown as area P in Fig. 1. The microstructure of the material solidified on the crucible was examined using an optical microscope and EDS/SEM, along with the sample poured out from the crucible. The optical micrographs of the sample from the crucible wall are given in Fig. 5. A layer containing a high density of particles was formed in the solid, as shown in Fig. 5a. The layer had a thickness of up to about 2 mm, depending on the location of the sample. The optical micrographs of the cross-section normal to the surface and parallel to the bottom edge are demonstrated in Fig. 5b–d. The particle size varied in a wide range, from a few μm to over 100 μm, as shown in Fig. 5c and d, respectively. A closer inspection of the large particles revealed that they were agglomerates of smaller ones. A typical EDS spectrum of the particle and the element distribution around it are shown in Fig. 6. Compared with the surrounding matrix, the particle was rich in Al and N, as illustrated by the brighter areas in contrast to the darker ones. A quantitative EDS analysis revealed that the average composition of these particles was 51.6 wt.% Al–33.2 wt.% Mg–13.9 wt.% N–1.3 wt.% O. The detected composition of the particle does not match the stoichimetry of AlN, which might have resulted from the limitation of the EDS analysis on light elements, such as nitrogen and carbon, and the involvement of the matrix in the analysis.

In order to further confirm the formation of AlN in the Mg–Al alloy, the particles in the sample shown in Figs. 5 and 6 were extracted in a 10 vol.% acetic acid ethanol solution and subjected to X-ray diffraction. The X-ray spectrum shown

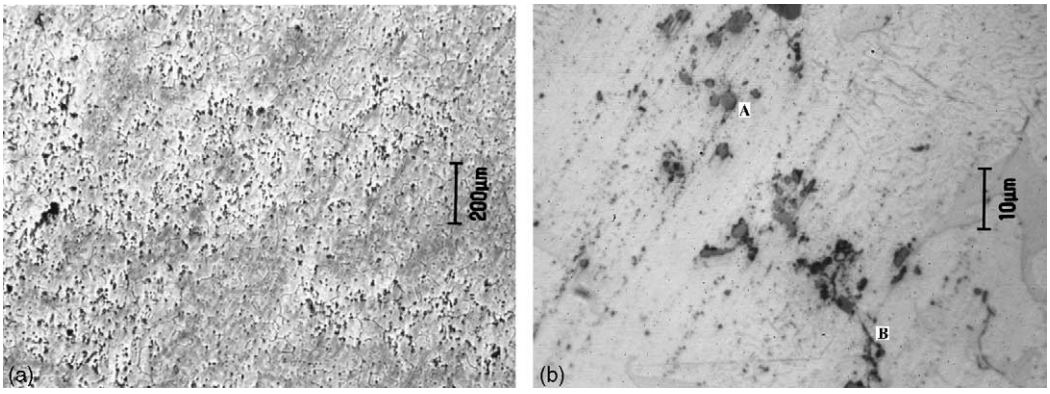

Fig. 4. Optical micrographs of the Mg–12.5 wt.% Al sample melted at 700 °C.

Table 1
Compositions of particles in Mg–12.5 wt.% Al samples melted at different temperatures

Temperature (°C)	Al (wt.%)	Mn (wt.%)	Ni (wt.%)	Fe (wt.%)	Mg (wt.%)
620	31.0	13.7	1.2	–	Balance
700	38.2	16.7	4.1	2.2	Balance
800	45.9	7.9	2.1	39.0	Balance

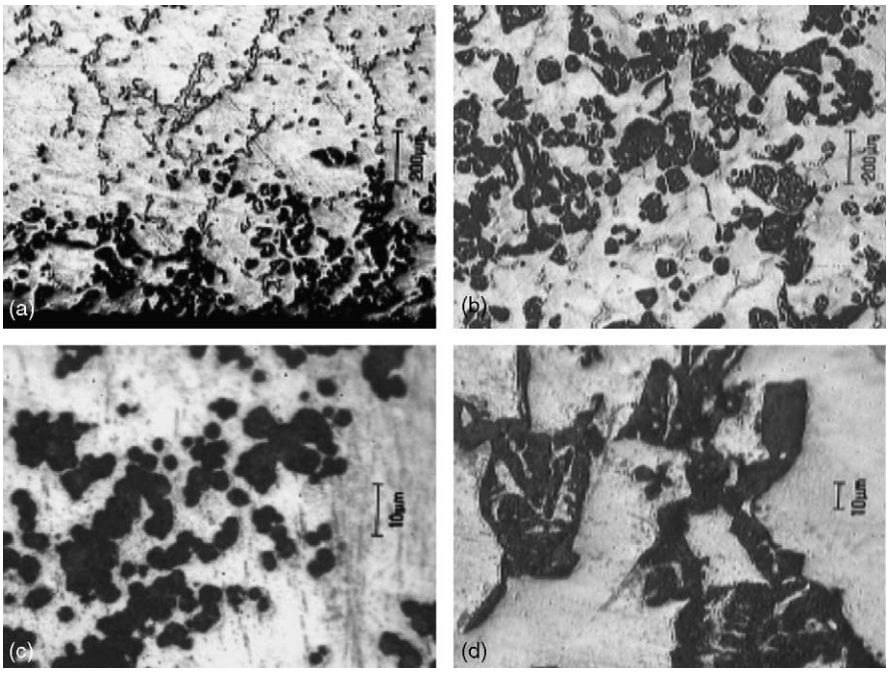

Fig. 5. Optical micrographs of the Mg–12.5 wt.% Al sample melted at 800 °C and solidified in the top portion of the melting crucible.

in Fig. 7 clearly demonstrates the in situ formation of AlN particles in Mg–Al melt during liquid nitridation at 800 °C.

The optical micrograph of the poured ingot melted at 800 °C is shown in Fig. 8. The particle-free areas of the sample had an average composition of 94.7 wt.% Mg–5.3 wt.% Al. As compared to the samples melted at 620 °C and 700 °C, the samples melted at 800 °C had a lower Al content in the matrix, which is likely due to the formation of AlN particles in the melt. The sample cast at 800 °C had fewer dark particles. However, as shown in Fig. 8b, these particles were much larger in size, up to 40 μm in maximum dimension for each single particle. As listed in Table 1 by the EDS analy-

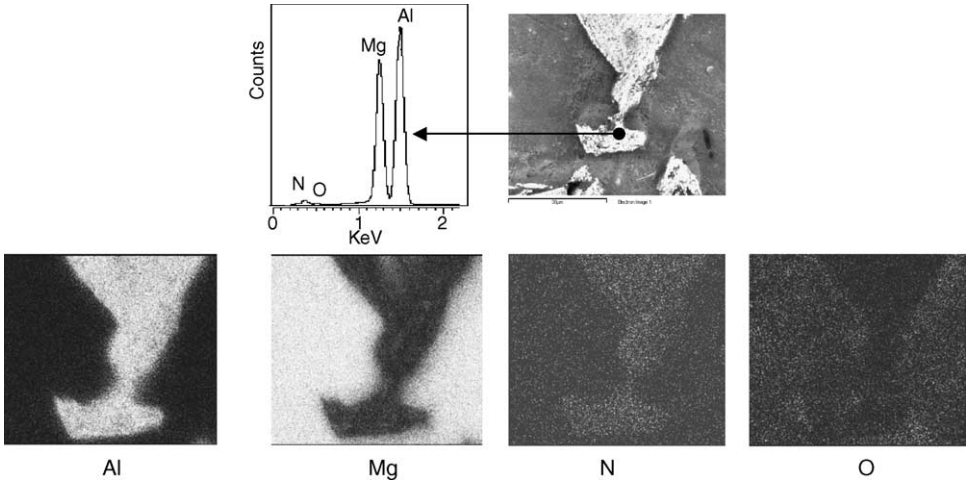

Fig. 6. EDS spectrum of a particle in the sample shown in Fig. 5 and corresponding mapping of Al, Mg, N, and O distribution around the particle.

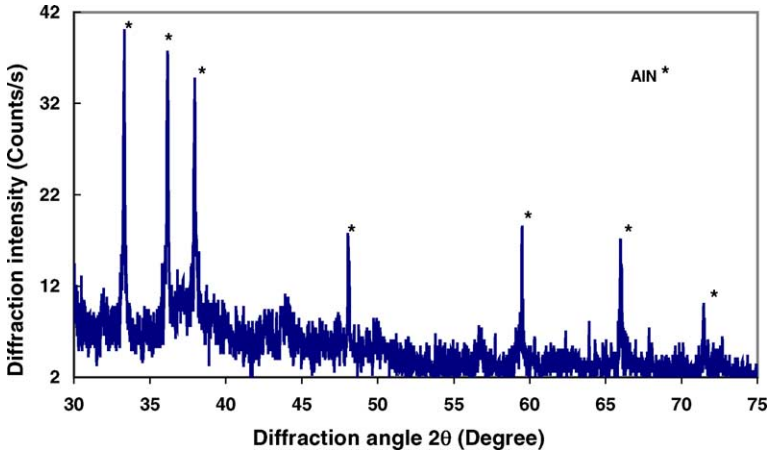

Fig. 7. XRD pattern (Cu Kα) of the extracted particles from the sample shown in Fig. 5.

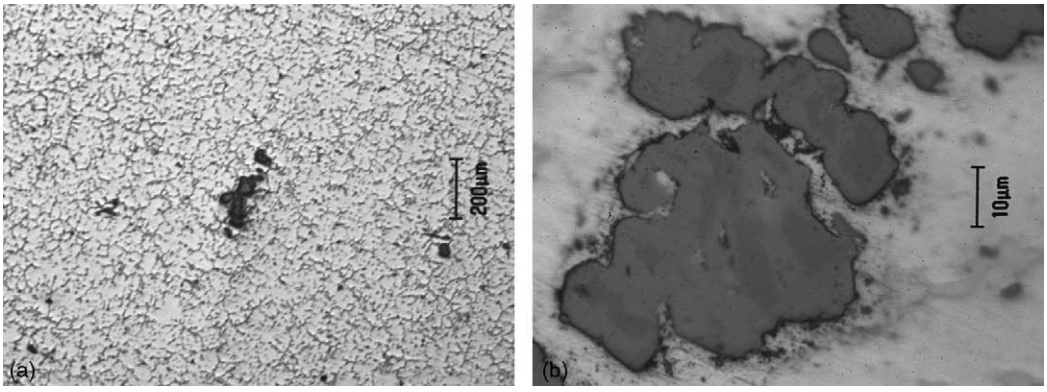

Fig. 8. Optical micrographs of the central area in the Mg–12.5 wt.% Al sample melted at 800 °C.

Table 2
EDS composition of particles in samples of different Al contents melted at 700 °C

Sample	Al (wt.%)	Mn (wt.%)	Ni (wt.%)	Fe (wt.%)	O (wt.%)	Mg (wt.%)
Mg–6 wt.% Al	34.7	31.9	9.7	4.7	1.0	Balance
Mg–10 wt.% Al	34.8	22.7	6.9	3.1	–	Balance
Mg–15 wt.% Al	34.6	30.7	25.1	–	1.0	Balance

sis, the particle contained a significant amount of Fe, along with Al, Mn, and Mg. The Fe most likely came from the melting steel crucible and the stainless steel thermocouple tubing.

3.2. Influence of Al content

The optical micrographs of the Mg alloys with 6 wt.%, 10 wt.%, and 15 wt.% of Al are shown in Fig. 9. It can be seen that increasing Al content in Mg–Al melt promoted the formation of the segregated particles. The composition of the segregated particles shown in Fig. 9b, d, and f was analyzed with SEM/EDS. The results are shown in Table 2. Similar to the Mg–12.5 wt.% Al sample melted at 700 °C, the particles in all the three samples were intermetallics containing Al, Mn, Ni, and Mg. No AlN particle was detected in the samples regardless of Al content.

4. Discussion

The experimental results demonstrated that AlN particles could be formed in situ by liquid nitridation in a Mg–Al alloy. A major difference in the nitridation process in a Mg–Al melt and an Al–Mg melt is the role of direct nitridation $2Al + N_2 \rightarrow 2AlN$. In an Al–Mg melt with a relatively low Mg concentration, the reaction of $2Al + N_2 \rightarrow 2AlN$ takes place in a certain temperature range, even though this process cannot proceed thoroughly because of the surface passivation of aluminium [11]. Increasing Mg content in the Al melt, however, serves two objectives. First, Mg decreases the surface tension of the aluminum melt and reduces Al_2O_3 on the surface of Al, thus promoting the break down of the passivation layer [11,15]; Secondly, Mg "catalyzes" the nitridation process through the formation of Mg_3N_2 powders. Thermodynamically, the direct nitridation of both Al and Mg is highly favorable, and

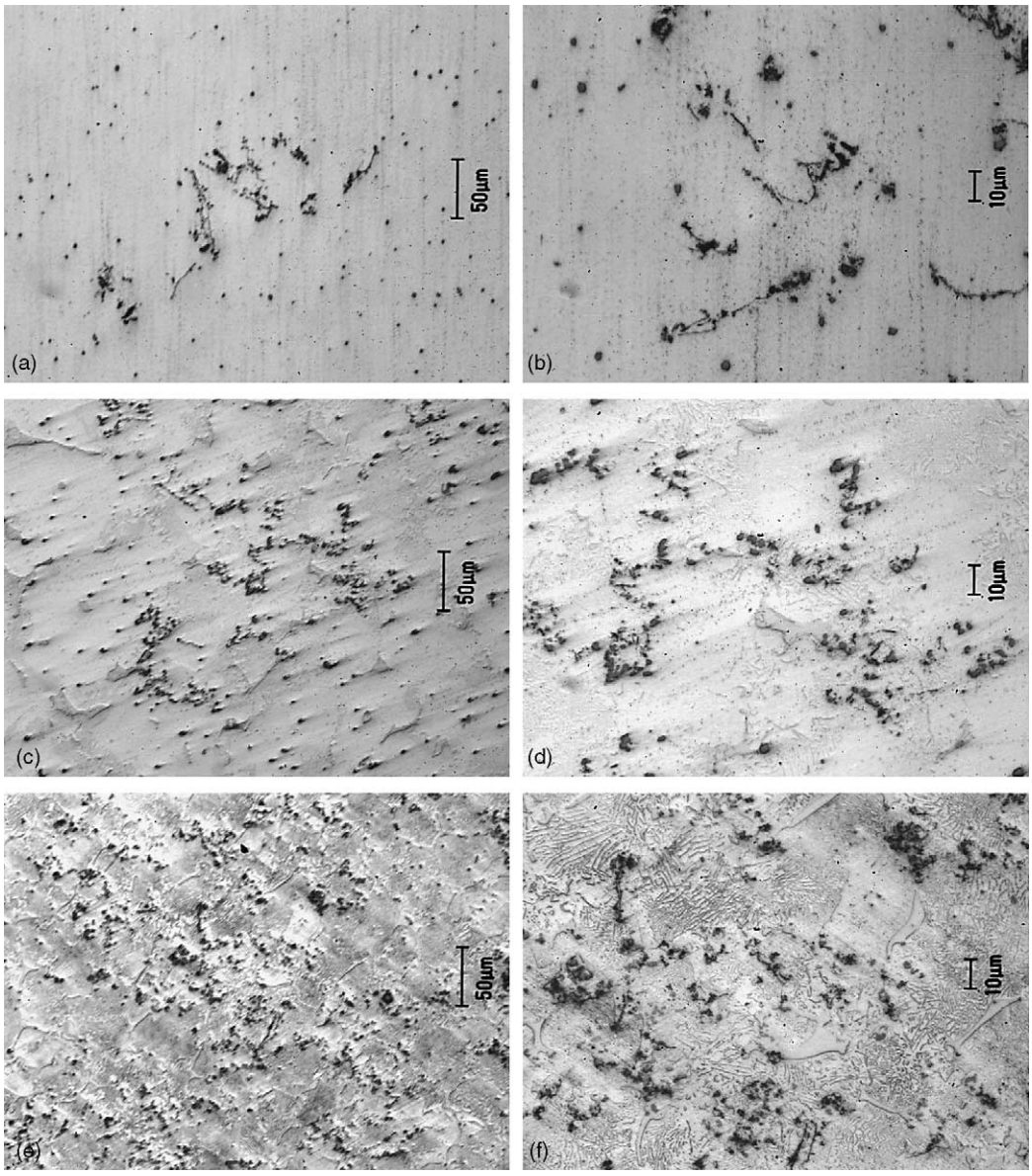

Fig. 9. Optical micrographs of the samples melted at 700 °C (a, b: 6 wt.%; c, d: 10 wt.%; e, f: 15 wt.%).

AlN has a greater stability than Mg_3N_2. However, the formation of Mg_3N_2 is much more kinetically favorable than that of AlN because the reaction takes place in the vapor phase [11]. Therefore, the presence of Mg facilitates the nitridation process through the indirect route. In short, both direct and indirect nitridation processes exist in an Al–Mg melt.

However, the liquid nitridation processes conducted at 700 °C in the Mg–Al melt did not produce a detectable amount of AlN particles within the examined Al contents from 6 wt.% to 15 wt.%. At 800 °C, AlN particles are only present near the crucible wall on the top surface of the melt. Combined with the facts that nitrogen is bubbled through the melt and Mg_3N_2 is mainly formed in the gaseous phase on top of the melt, it can be concluded that AlN formation is mainly ascribed to the indirect nitridation process. The mechanism of AlN formation in the Mg–Al melt is believed to be similar to that in the Al–Mg alloys. During the melting process, Mg_3N_2 powders are first produced in the gaseous phase. Some of the Mg_3N_2 powders fall into Mg–Al melt, reacting with Al in the Mg melt to form AlN particles. Thus, AlN will form predominantly on the top surface layer of the melt. The relatively low wettability of AlN with molten Mg at these temperatures probably prevented AlN particles from settling down into the Mg–Al melt. Therefore, AlN particles are only found in the solid near the top of the melt. The nitridation process is also temperature-dependent. A higher temperature favors the formation of AlN. The results demonstrate the feasibility of in situ forming AlN reinforcements in a Mg–Al melt by liquid nitridation. However, further research work is needed to control the AlN particle size and distribution in the magnesium matrix composites.

Another important feature of liquid nitridation in a Mg–Al melt is that a much lower melting temperature is needed for the process to occur as compared to an Al–Mg melt. The ease of Mg_3N_2 formation is believed to be the major contributing factor for the difference. In Al–Mg alloys, it has been revealed that AlN cannot be formed until the melting temperature reaches at least 900 °C [12,16]. In addition, the minimum nitridation temperature in a molten Al–Mg alloy greatly depends on the Mg content. Under a N_2 pressure of 1 MPa, the minimum nitridation temperatures were around 1300 °C, 1180 °C, and 1090 °C, for Al alloys with a magnesium content of 1.96%, 3.98%, and 4.85%, respectively [12]. The relatively low content of Mg in Al–Mg alloys necessitates the high temperature to produce a sufficient amount of Mg_3N_2 phase for the liquid nitridation reactions to occur. Compared with the industrial melting practices for Al–Mg alloys, the nitridation temperature is too high to be used in practical manufacturing. In the Mg–Al system, on the other hand, the dominating concentration of Mg greatly lowers the temperature required for producing a sufficient amount of magnesium vapor for the formation of Mg_3N_2 powders. Mg–Al alloys are commonly melted at around 650 °C–700 °C. The current study has shown the formation of a significant amount of Mg_3N_2 powder at 700 °C and a large amount of Mg_3N_2 powder at 800 °C. With further optimization of the process parameters such as melting time, and N_2 gas pressure, the nitridation temperature could be further reduced. Therefore, the liquid nitridation temperature in the Mg–Al alloys is much closer to that used in industrial melting practice as compared to the Al–Mg alloys.

5. Summary

AlN can be in situ formed in Mg–Al melt by a liquid nitridation process. The key mechanism for the formation of AlN is the catalyzed process of $N_2 + 3Mg \rightarrow Mg_3N_2$ and $Mg_3N_2 + 2Al \rightarrow 2AlN + 3Mg$. The high concentration of Mg in Mg–Al results in a much lower temperature for the occurrence of liquid nitridation than in Al–Mg melt. The Al content is less critical than the temperature for the initiation of the nitridation process in Mg–Al melt.

Acknowledgements

The authors wish to thank Moe Islam for his valuable discussions in the course of this research work. The assistances from David Arnold, Mike Meinert, Jianying Chen, and Shenghui Wang in conducting the experiments are also gratefully acknowledged.

References

[1] A. Luo, Metall. Mater. Trans. A 26A (September) (1995) 2445.
[2] K. Wu, M. Zheng, M. Zhao, C. Yao, J. Li, Scripta Materialia 35 (4) (1996) 529–534.
[3] M. Zarinejad, S. Firoozi, P. Abachi, K. Purazrang, Canadian Institute of Mining, Metallurgy and Petroleum, Metal /Ceramic Interactions, Canada, 2002, pp. 191–203.
[4] M. Mabuchi, K. Kubota, K. Higashi, J. Mater. Sci. 31 (1996) 1529–1535.
[5] M. Mabuchi, K. Kubota, K. Higashi, Mater. Lett. 19 (1994) 247–250.
[6] M. Mabuchi, K. Kubota, K. Higashi, Minerals, Metals and Materials Society/AIME, USA, 1995 pp. 463–470.
[7] T. Choh, M. Kobashi, H. Nakata, H. Kaneda, Mater. Sci. Forum 217–222 (1) (1996) 353–358.
[8] K. Yamada, T. Takahashi, M. Motoyama, J. Jpn. Inst. Met. (Jpn.) 60 (1) (1996) 100–105.
[9] M.A. Matin, L. Lu, M. Gupta, Scripta Materialia 45 (4 Aug. 31) (2001) 479–486.
[10] H. Scholz, P. Greil, J. Mater. Sci. 26 (Feb.1) (1991) 669–677.
[11] Q. Hou, R. Mutharasan, M. Koczak, Mater. Sci. Eng. A 195 (1995) 121–129.
[12] S. Kudela, A. Schweighofer, Kovove Materialy 17 (6) (1979) 724–737.
[13] H. Lehuy, S. Dallaire, Processing of Ceramic and Metal Matrix Composites, Halifax, Nova Scotia, Canada, 1989, pp. 302–311.
[14] H.Z. Ye, X.Y. Liu, B. Luan, Mater. Lett. 58 (19) (2004) 2361–2364.
[15] B. Srinivasa Rao, V. Jayaram, Acta Mater. 49 (2001) 2373–2385.
[16] S. Swaminathan, B. Srinivasa Rao, V. Jayaram, Acta Mater. 50 (2002) 3093–3104.